International Journal of Nanomedicine Dovepress

Open Access Full Text Article ORIGINAL RESEARCH

SFRP1-Silencing GapmeR-Loaded Lipid-Polymer Hybrid Nanoparticles for Bone Regeneration in Osteoporosis: Effect of Dosing and Targeting Strategy

Erik Briffault[1,2], Ricardo Reyes[2,3], Patricia Garcia-Garcia[1,2], Helena Rouco[1], Luis Diaz-Gomez[4], Maria Rosa Arnau[2,5], Carmen Evora[1,3], Patricia Diaz-Rodriguez[2,4], Araceli Delgado[1,2]

[1]Department of Chemical Engineering and Pharmaceutical Technology, Universidad de La Laguna, La Laguna, 38206, Spain; [2]Institute of Biomedical Technologies (ITB), Universidad de La Laguna, La Laguna, 38320, Spain; [3]Department of Biochemistry, Microbiology, Cell Biology and Genetics, Universidad de La Laguna, La Laguna, 38200, Spain; [4]Department of Pharmacology, Pharmacy and Pharmaceutical Technology, I+D Farma Group (GI-1645), Facultad de Farmacia, Instituto de Materiales (iMATUS) and Health Research Institute of Santiago de Compostela (IDIS), Universidade de Santiago de Compostela, Santiago de Compostela, 15782, Spain; [5]Servicio de Estabulario, Universidad de La Laguna, La Laguna, 38206, Spain

Correspondence: Patricia Diaz-Rodriguez; Araceli Delgado, Email patricia.diaz.rodriguez@usc.es; adelgado@ull.edu.es

Introduction: Osteoporosis is a metabolic disorder characterized by the loss of bone mass and density. Nucleic acid-based therapies are among the most innovative approaches for osteoporosis management, although their effective delivery to bone tissue remains a challenge. In this work, SFRP1-silencing GampeR loaded-nanoparticles were prepared and functionalized with specific moieties to improve bone targeting and, consequently, therapeutic efficacy. SFRP1-silencing would promote osteoblastic differentiation by enhancing the WNT/β-catenin pathway and thus diminishing the progression of osteoporosis.

Methods: A nucleic acid-based delivery system consisting of lipid-polymer hybrid nanoparticles (LPNPs) loading a GapmeR for SFRP1 silencing was developed and further functionalized with two bone-targeting moieties: a specific aptamer (Apt) for murine mesenchymal stem cells and an antiresorptive drug, namely alendronate (ALD). These systems were tested in vivo in osteoporotic mice at different dosage regimens to analyze dose dependence in bone-forming activity and potential toxicity. The quality of trabecular and cortical bone was assessed by both micro computed tomography (micro-CT) and histological and histomorphometric analyses. Early and late osteogenesis were quantified by immunohistochemistry.

Results: Results showed that functionalizing LPNPs loaded with an SFRP1-silencing GapmeR using both Apt and ALD improved bone quality and enhanced osteogenesis following a dose–effect relationship, as revealed by micro-CT, histological and immunohistochemical analyses. In contrast, non-functionalized LPNPs did not produce these effects.

Conclusion: These findings highlight the relevance of proper targeting and dosage in nucleic acid-based therapeutics, proving to be crucial for exerting their therapeutic effect: a deficient targeting strategy and/or dosage may result in the therapeutic failure of an adequate gene therapy agent.

Keywords: osteoporosis, bone targeting, nanoparticle dose-effect, gene therapy, aptamer, alendronate, micro-CT

Introduction

Despite the vast efforts and resources focused on the stimulation of bone formation in systemic bone-related pathologies such as osteoporosis, the improvement of the osseous tissue quality remains challenging.[1] The associated diminished bone strength and stiffness increases the risk of bone fractures after low-energy injuries leading to fragility fractures. These fractures represent an economic burden and are only going to become an ever-increasing problem with the aging of the population. Just in 2010 fragility fracture treatment represented 22.42 billion euros in Europe.[2] Moreover, the established pro-degradative environment that imbalances the normal tissue homeostasis impairs bone formation, thus increasing the risk of non-union bone fractures and implant failure.[3–8] Different strategies have been screened in order to

Received: 2 May 2024
Accepted: 5 November 2024
Published: 20 November 2024

Graphical Abstract

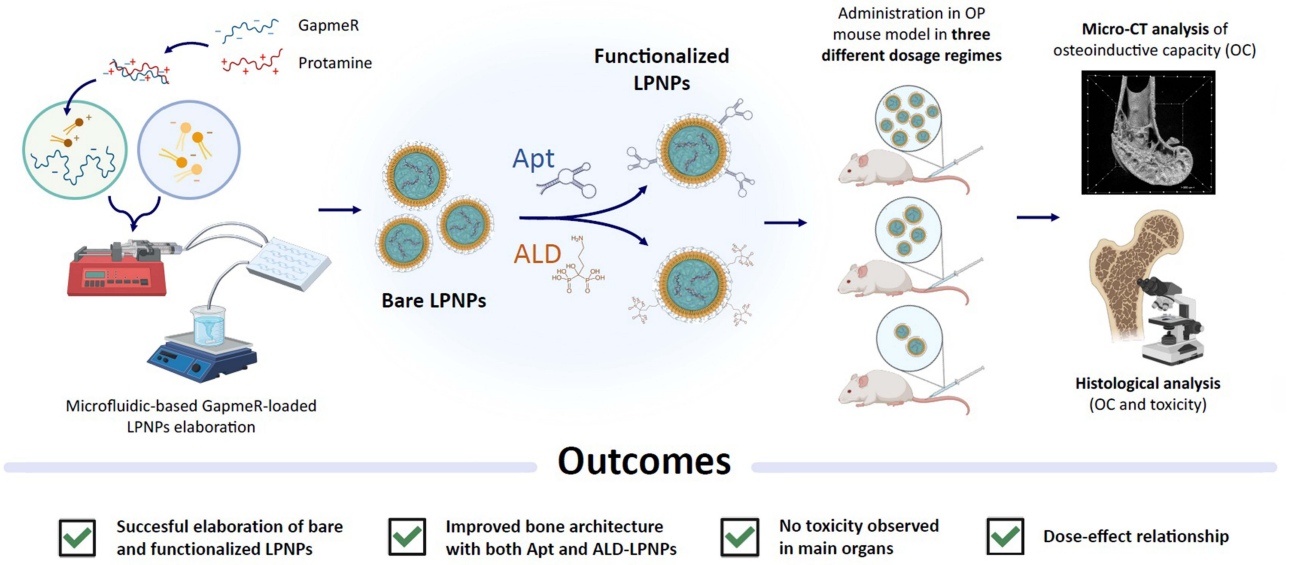

counterbalance this situation, including antiresorptive drugs such as bisphosphonates and RANKL inhibitors or anabolic molecules such as teriparatide, abaloparatide and romosozumab.[9] However, significant drawbacks such as osteonecrosis of the jaw and atypical femoral fractures, frequently described in patients with high-dose or long-term treatments, have limited the use of these therapeutic molecules.[10]

Improvements in the nucleic acid-based therapeutic stability and the high throughput discovery of genetic targets have exponentially increased the potential of oligonucleotide therapies to correct or modify cell function.[11] Gene therapy strategies are designed to induce the expression of the gene of interest or to reduce or modify protein expression by gene silencing. Osteoporosis has not been an exception in the development of gene silencing therapeutic strategies, and several small interfering RNAs (siRNA) and artificial microRNAs (miRNAs) have been developed aiming at improving bone quality mainly by controlling the WNT/β-catenin pathway. This target route is selected based on its role in the commitment of mesenchymal stem cells (MSCs) towards osteoblastic differentiation and the control over osteoclasts maturation and differentiation.[12] The therapeutic efficacy of WNT/β-catenin pathway gene silencing strategies highly relies on the development of suitable carriers able to ensure their stability, cell uptake (transfection), and ideally, targeting.[13] In this way, viral vectors have been loaded with miRNAs designed to silence the expression of the WNT inhibitors sclerostin and schnurri-3. The intravenous administration of these systems led to an enhancement in bone mass in osteoporotic mice associated with an enhancement in the osteoblast activity, showing better results when both inhibitors were silenced.[14,15] Similarly, schnurri-3 siRNA has been loaded into extracellular vesicles and intravenously injected into osteoporotic mice, increasing bone formation.[16] In alignment with this, GLG1-expressing extracellular vesicles have also been used to carry Wnt agonist 1 and deliver it specifically to bone tissue, satisfactorily achieving increased bone formation and fracture healing in mice.[17] Additionally, mesoporous silica nanoparticles have been loaded with sclerostin siRNA and injected into osteoporotic animals promoting an improvement in bone architecture and recovering the bone mineral content.[18] Along the same lines, a modified Runx2 mRNA-loaded lipid nanoparticle-based delivery system, functionalized with zoledronic acid to target bone tissue, has been developed, significantly enhancing bone repair and osteogenesis in both osteoporotic and bone defect mouse models.[19]

Another strategy used in gene therapy to manage osteoporosis is the suppression of bone resorption by silencing genes related to osteoclasts multinucleation and function. In this regard, liposomes functionalized with Asp8 peptide and loaded with antagomir-148a, able to suppress the osteoclastogenic miR-148 a, have been developed. The systems were

administered once per week for six weeks to osteoporotic mice, leading to a decrease in the osteoclast number.[20] The same osteoclasts-targeting peptide was used to target polymeric nanoparticles to osteoclasts but designed to silence semaphorin 4D. The treatment with these systems led to the recovery of bone mass in osteoporotic mice.[21] However, the translation of the developed therapies requires a more profound understanding of the possible dose–response effects together with the establishment of suitable dosage and targeting strategies.

Current bone gene therapy strategies based on oligonucleotide loaded nanoparticles of diverse compositions are administered following variable dosage approaches, ranging from a single dose for six weeks of experiment to an injection every two days for 2 or 3 weeks of treatment. Additionally, the selected doses are quite different and expressed using diverse nomenclatures based on either the concentration of nanoparticles in number or mass per volume, the number of genome copies for studies performed with viral vectors, or the amount of antisense oligonucleotide. The variability between studies complicates comparisons and hinders the establishment of adequate dose and dosage intervals. Therefore, the main objective of this study is to elucidate the effect/toxicity of antisense oligonucleotide dose, dosage time and targeting strategy over the bone formation induction of ASOs-loaded nanoparticles designed to control the WNT/β-catenin pathway. To this end, nanoparticulated systems previously designed to encapsulate a GapmeR will be functionalized with two different moieties.

In a previous study, we developed lipid/polymer hybrid nanoparticles functionalized with a bone-specific aptamer able to successfully load an ASO against SFRP1.[22] This protein acts as a WNT/β-catenin pathway antagonist decreasing osteoblast survival and inducing osteoporosis progression.[23] The therapeutic nanoparticles showed an enhancement in bone synthesis when compared to functionalized controls. Moreover, an improvement in the bone formation was observed in osteoporotic mice treated with these nanoparticles. Despite the promising results obtained, only one dosage strategy of a monthly administration for 3 months was used and only one targeting moiety was evaluated. Therefore, the present study explores the potential dose-effect of the developed nanoparticles and the outcome of variable dosage approaches on bone formation and toxicity. Additionally, differently from our previous work and moving forward towards the translation of the systems, the formulations were prepared by a microfluidic-based system to enable continuous manufacturing. This transition required the optimization of the synthesis procedure and the fine tuning of the composition. The developed systems were then functionalized by covalent bonding using two different targeting molecules: the murine bone marrow MSCs-specific aptamer already tested on the previous experiment[22] and alendronate, a bisphosphonate with an already known affinity for the bone extracellular matrix, previously used as a targeting moiety for nanoparticulated systems.[9,24] This approach aimed to test a different combination of dosage regimen and functionalization strategy that might outperform the results achieved with the aptamer at one specific dosage. This information is key in the clinical translation of the developed systems and further understanding the dose-effect of gene therapy strategies. Both functionalized systems were compared against a non-functionalized control at identical dosage regimens. The capacity of the therapeutic nanoparticles to induce bone formation was analyzed by micro-CT and histological evaluation. Additionally, the toxicity of the treatments on major organs was studied through histological analysis.

Materials and Methods

Reagents

Poly(D,L-lactide-co-glycolide) (PLGA) (Resomer RG502H, Mw 7000–17,000) was obtained from Evonik (Germany), soy L-α-phosphatidylcholine (95%) (lecithin) was purchased from Avanti Polar Lipids (USA). DOTAP (1,2-dioleoyl-3-trimethylammonium-propane), protamine sulfate (Mw 5000–10,000), Tris(2-carboxyethyl)phosphine hydrochloride (TCEP) and alendronate sodium (ALD) were provided by Sigma-Aldrich (USA). 1,2-distearoyl-sn-glycero-3-phosphoethanolamine-N-[methoxy(polyethylene-glycol)-2000] (DSPE-mPEG$_{2000}$); 1.2-distearoyl-sn-glycero-3-phosphoethanolamine-N-[maleimide(polyethyleneglycol)-2000] (DSPE-PEG$_{2000}$-MAL) and 1.2-distearoyl-sn-glycero-3-phosph oethanolamine-PEG-succinimidyl ester (DSPE-PEG$_{2000}$-NHS) were obtained from Nanosoft Polymers (USA). O-phthalaldehyde and 2-mercaptoethanol were purchased from Sigma-Aldrich (USA). Dexamethasone 21-isonicotinate (Deyanil Retard) was obtained from Fatro Ibérica, Spain. Ethanol and Paraplast® were purchased from Panreac (Spain).

The specific SFRP1-silencing GapmeR (5′-GGTCAGTAACTAAGTT-3′) and control GapmeR without therapeutical activity (5′-AACACGTCTATACGC-3′), labelled or not with FAM, were designed and purchased from Qiagen (Germany). The thiol modified aptamer for murine mesenchymal stem cells (SS-Apt) (5′-GAATTCAGTCGGACAGCGA CGA CGGTGATATGTCAAGGTCGTATGCACGAGTCAGAGGGATGGACGAATATCGTCTCCC-/3ThioMC3-D/-3′) was obtained from Integrated DNA Technologies (USA).

Preparation of Lipid-Polymer Hybrid Nanoparticles

GapmeR-loaded lipid polymer hybrid nanoparticles (LPNPs) were synthetized by the nanoprecipitation method using a microfluidic system. The composition of the nanoparticles was tuned to obtain systems with adequate physicochemical properties based on the previously developed formulations elaborated by bulk nanoprecipitation.[22] Non-functionalized NPs (NF-LPNPs) were obtained by mixing an organic phase containing PLGA (2.5 mg/mL) and DOTAP (0.15 mg/mL) in acetonitrile at 500 µL/min flow rate with an aqueous phase containing lecithin (16 µg/mL) and DSPE-mPEG$_{2000}$ (55 µg/mL) in ethanol 4% at 3 mL/min flow rate. The lecithin solution was previously heated to 65°C until dissolution, and both solutions were filtrated through 0.45 µm syringe filters prior to their loading in the microfluidics system. The mixing process was developed on a Micromixer chip (Part N° 3200401, Dolomite microfluidics, UK) using a Mitos-Duo-XS-Pump (Dolomite microfluidics, UK) and a syringe pump (model 569, KD Scientific, USA). The resulting formulations were collected in a beaker considering batches of two minutes flow and kept under stirring for two hours to ensure acetonitrile evaporation. After this time, non-incorporated components were removed by ultrafiltration through 100 kDa MWCO filters (Millipore Amicon, USA) at 10,000 rpm for 10 min. The purified nanoparticles were then washed and resuspended in Milli-Q water.

The composition of the aqueous phase was modified to allow for the functionalization of the nanoparticles. In the case of the murine mesenchymal stem cell aptamer (Apt-LPNPs) functionalization, DSPE-PEG$_{2000}$-MAL was added to the aqueous phase replacing an equivalent amount of DSPE-mPEG$_{2000.}$ Therefore, the composition of the aqueous phase was: lecithin (16 µg/mL), DSPE-mPEG2000 (44.7 µg/mL) and DSPE-PEG$_{2000}$-MAL (10.3 µg/mL). For the alendronate (ALD) functionalization (ALD-LPNPs), DSPE-PEG$_{2000}$-NHS was incorporated into the aqueous phase removing an equivalent amount of DSPE-mPEG$_{2000}$. Hence, the composition of the aqueous phase was as follows: lecithin (16 µg/mL), DSPE-mPEG2000 (41.2 µg/mL) and DSPE-PEG$_{2000}$-NHS (13.8 µg/mL).

To obtain GapmeR loaded nanoparticles, the oligonucleotide was previously condensed with protamine in a 1:45 GapmeR to protamine mass ratio for 40 minutes, and afterwards, this solution, containing 20 µg/mL GapmeR, was injected into the organic phase at 50 µL/mL. Two GapmeRs were used, either SFRP1-silencing GapmeR or control GapmeR.

NPs Surface Modification for Bone Targeting

NPs surfaces were functionalized either with a specific aptamer (Apt) for bone marrow murine MSCs or with ALD to target bone tissue. Both molecules were incorporated to the NPs surface via a covalent link. For the aptamer functionalization (Apt-LPNPs), a 3'disulfide bond-modified single-strand DNA aptamer was used as previously reported.[25] Prior to reaction, the SS bond was reduced to SH by incubation with a 100-fold higher amount of tris(2-carboxyethyl) phosphine (TCEP) for 1 h. NPs prepared as described in Section 2.2 were buffered with 5X phosphate buffer until a final pH of 7.4. The reactive Apt solution was then added to the NPs formulation using an Apt:MAL molar ratio of 1:100 previously optimized.[25] Suspensions were incubated for 1 h at room temperature to allow for the reaction of the maleimide groups present in DSPE-mPEG$_{2000}$-MAL with the thiol groups of the Apt.

To prepare NPs-ALD, NPs elaborated containing DSPE-PEG$_{2000}$-NHS were diluted in 5-fold concentrated HEPES 1M (Corning, USA) to achieve a pH of 7.4. After this, the required volume of an aqueous solution of ALD (2 mg/mL) was added to obtain different NHS:ALD molar ratios: 1:1, 1:2, 1:5 and 1:10. The LPNPs and ALD mixture was incubated for 1 h at room temperature to allow for the reaction of the NHS moiety of modified lipids with the NH_2 group of ALD. To assess the ALD association efficiency (AE), non-incorporated ALD was quantified using a spectrophotometric derivatization method. Consequently, NPs were centrifuged using 10 kDa MWCO filters (Millipore Amicon, USA) and the filtrate was collected and

mixed with o-phthalaldehyde and 2-mercaptoethanol as previously reported.[26] The derivate product was quantified at 334 nm (Ultrospect 3300pro, Biochrom, England). The association efficiency was calculated as follows:

$$AE(\%) = \frac{A_{total\ derivate} - A_{free\ derivate}}{A_{total\ derivate}}.100$$

where $A_{total\ derivate}$ is the absorbance of a solution of ALD at the functionalization concentration after derivatization and $A_{free\ derivate}$ is the absorbance of the collected non-linked ALD after derivatization.

LPNPs Characterization

All nanoparticles (NF-LPNPs, Apt-LPNPs, and ALD-LPNPs) before and after functionalization, when applicable, were characterized in terms of size (average hydrodynamic diameter (Z-size) and polydispersity index (PdI)) and ζ-potential (ZP) by dynamic light scattering (DLS) and electrophoretic light scattering (ELS), respectively, using a Zetasizer Nano ZS (Malvern Panalytical Ltd., UK). These measurements were performed in triplicate after dilution in Milli-Q water. NPs were also characterized by nanoparticle tracking analysis (NTA) after dilution in Milli-Q water (Nanosight NS300, Malvern Panalytical Ltd., UK). The encapsulation efficiency of the developed lipid-polymer nanoparticles was assessed using a FAM-labelled control GapmeR by determining the non-encapsulated GapmeR. To this end, after NPs ultrafiltration with 100 kDa MWCO filters (Amicon®Ultra, USA), the filtrate was collected and the fluorescence was measured using a plate reader (Biotek, USA) at 485/528 nm.

In vivo Experiments

Animal experiments were carried out in conformity with the EC directive on Care and Use of Animals (2010/63/UE) and with the approval by the Ethics Committee for animal care of University of La Laguna Experimental Procedures (CEIBA2018-0310). All surgical procedures were carried out under aseptic conditions.

Osteoporosis Animal Model

Osteoporosis was induced in 16-week-old female FVB mice as previously established.[26] Briefly, bilateral ovariectomy (OVX) was performed on 100 mice under inhalation anesthesia (isoflurane, ISOFLO®). Two weeks after ovariectomy, a 3 mg/kg dose of dexamethasone 21-isonicotinate was administered subcutaneously, and the same procedure was repeated weekly for 4 months. Analgesia consisted of subcutaneously administered buprenorphine (0.01 mg/kg) before surgery and paracetamol in water (70 mg/kg) for 3 days after the intervention.

In vivo Osteoinduction Capacity

To analyze the osteoinduction capacity of SFRP1-silencing GapmeR-loaded NPs, osteoporotic mice were randomly divided into different groups. Nanoparticles dispersions or controls (50 µL) were systemically administered through the tail vein using three different dosage regimens; A) Hybrid nanoparticles carrying 25 ng of GapmeR were injected once a month for three months, B) Hybrid nanoparticles carrying 25 ng of GapmeR were injected every two weeks for three months or C) Hybrid nanoparticles carrying 50 ng of GapmeR were injected every two weeks for three months. Therefore, mice received a final dose of 75 ng, 150 ng or 300 ng of the oligonucleotide. These three strategies were tested using the therapeutic GapmeR loaded nanoparticles (SFRP1) and control GapmeR loaded nanoparticles (Cntrl). Moreover, untargeted hybrid nanoparticles (NF-LPNPs) or nanoparticles functionalized by the two targeting strategies (ALD-LPNPs, Apt-LPNPs) were tested. Additionally, mice treated with the same volume (50 µL) of saline solution every two weeks (SS2W) or every four weeks (SS4W) were used as controls. Therefore, animals were divided into 20 experimental groups (n = 5) as described in Table 1.

After three months of treatment, mice were euthanized under isoflurane anesthesia and then fixed by intracardiac perfusion with 4% paraformaldehyde (PFA).[27] Both femurs were collected to analyze bone structure by histological, histomorphometric and immunohistochemistry (collagen type I and osteocalcin) analyses and micro-computed tomography (micro-CT) using one for each technique. Moreover, main organs (liver, kidneys, spleen, lungs, heart, brain, and popliteal and inguinal ganglions) were extracted for histological analyses to assess toxicity.

Table 1 Experimental Groups Tested

Nomenclature (Group #)	GapmeR	Dose (ng)	Functionalization	Time-Interval
NF-LPNPs-SFRP1 (1)	SFRP1	75	–	4 weeks
NF-LPNPs-SFRP1 (2)	SFRP1	150	–	2 weeks
NF-LPNPs-SFRP1 (3)	SFRP1	300	–	2 weeks
ALD-LPNPs-SFRP1 (4)	SFRP1	75	ALD	4 weeks
ALD-LPNPs-SFRP1 (5)	SFRP1	150	ALD	2 weeks
ALD-LPNPs-SFRP1 (6)	SFRP1	300	ALD	2 weeks
Apt-LPNPs-SFRP1 (7)	SFRP1	75	Apt	4 weeks
Apt-LPNPs-SFRP1 (8)	SFRP1	150	Apt	2 weeks
Apt-LPNPs-SFRP1 (9)	SFRP1	300	Apt	2 weeks
NF-LPNPs-Cntrl (10)	Control	75	–	4 weeks
NF-LPNPs-Cntrl (11)	Control	150	–	2 weeks
NF-LPNPs-Cntrl (12)	Control	300	–	2 weeks
ALD-LPNPs-Cntrl (13)	Control	75	ALD	4 weeks
ALD-LPNPs-Cntrl (14)	Control	150	ALD	2 weeks
ALD-LPNPs-Cntrl (15)	Control	300	ALD	2 weeks
Apt-LPNPs-Cntrl (16)	Control	75	Apt	4 weeks
Apt-LPNPs-Cntrl (17)	Control	150	Apt	2 weeks
Apt-LPNPs-SFRP1 (18)	Control	300	Apt	2 weeks
SS2W (19)	–	–	–	2 weeks
SS4W (20)	–	–	–	4 weeks

Micro-CT Analysis

Micro-Computed tomography (micro-CT) was performed to analyze qualitatively and quantitatively the bone structure at the end point of analysis (3 months after the initial administration). Femurs collected for micro-CT analysis were washed with distilled water, wrapped in gauze, soaked in saline physiological solution immediately after extraction and kept frozen until analysis.

Scan acquisition was carried out using a Skyscan 1272 micro-CT scanner (Bruker, Belgium). Data were acquired using a voxel size of 5 µm, 180° scan, filter Al 1 mm, voltage 80 kV and a current of 125 µA. The projections were reconstructed, resliced, and analyzed using NRecon and CTAn software (Bruker, Belgium). The scans were reconstructed using the optimal parameters specifically designed for this study, including a smoothing factor of 4, a ring artifact reduction of 10, a beam-hardening correction of 60%, and a misalignment compensation adjusted for each individual set. Bone Mineral Density (BMD) calibration phantoms (Bruker) with concentrations of Calcium Hydroxyapatite of 0.30 and 1.25 g/cm³ were used for density calibration. For trabecular bone, the distal femur epiphysis was selected for analysis within an adaptative region of interest (ROI) commencing at the growth plate and extending a further longitudinal distance of 1.5 to 2 mm, including the secondary spongiosa. Analyzed parameters include bone mineral density (BMD), Structure Model Index (SMI), bone volume/total volume (BV/TV), trabecular number (Tb.N), trabecular width (Tb.Wi), trabecular separation (Tb.Sp), cortical BMD and cortical width (Ct.Wi).

Bone Histological and Histomorphometrical Analysis

In order to perform histological and histomorphometrical analyses of the bone, the extracted femurs were kept in 4% PFA solution for 48 hours followed by decalcification in Histofix® Decalcifier (Panreac, Barcelona, Spain) and embedded in Paraplast®, as previously reported.[28] Longitudinal sections of 5 µm thick were obtained with a microtome (Shandon Finesse 325). The sections were stained with hematoxylin-erythrosine and Masson-Trichrome for bone structure evaluation. Sections were analyzed by light microscopy (LEICA DM 4000B) and computer-based image analysis software (Leica Q-win V3 Pro-Image Analysis System, Barcelona, Spain). The histomorphometric analysis was carried out by measuring the following parameters: width of the cortical bone (Ct.Wi) and number (Tb.N), width (Tb.Wi), and separation (Tb.Sp) of the trabeculae in cancellous bone. The histomorphometric parameters were evaluated in 2D as direct indexes, using 5 µm thick longitudinal sections throughout the entire femur. Between 8 and 12 sections per animal were evaluated. Trabeculae number (Tb.N) was quantified considering different trabeculae as those in different directions or orientations. Trabecular separation (Tb.Sp) was measured as the distance between the borders of the trabeculae. Trabecular width (Tb.Wi) and cortical bone width (Ct.Wi), were determined as the distance between the edges in each of these structures, measured at different longitudinal points. The dimensions of the structural parameters of the cancellous bone (Tb.N, Tb.Sp and Tb.Wi) were measured at epiphyseal regions, while the cortical bone structural measurements (Ct. Wi) were obtained in, epiphyseal and diaphyseal bone regions.

Immunohistochemistry Analysis

The expression of collagen type I (Col I), an early osteogenesis marker, and osteocalcin (OCN), a late osteogenesis and mineralization marker, were evaluated by immunohistochemical analysis. Briefly, sections were deparaffined and rehydrated in Tris-buffered saline (TBS) (pH 7.4, 0.01 M Trizma base, 0.04 M Tris hydrochloride, 0.15 M NaCl), also used for all further incubations and rinse steps. Sections were incubated in citrate buffer (pH 6) at 90 °C for antigen retrieval during 5 min. After a rinse step, sections were blocked with 2% FBS in TBS–0.2% Triton X-100 (blocking buffer). The immunohistochemical procedure was carried out by incubating the sections with Col I and OCN polyclonal antibodies (1/100) (Millipore, Spain) in blocking buffer at 4 °C overnight. Sections were rinsed three times, then incubated with biotin-SP-conjugated donkey anti-rabbit F(ab) fragment (1/200) (Millipore, Spain) in blocking buffer for 1 h followed by rinsing and then incubation in peroxidase conjugated streptavidin (1/300) (Millipore, Spain) for 1 h. Peroxidase activity was revealed in Tris–HCl buffer (0.05 M, pH 7.6) containing 0.005% w/v of 3.3-Diaminobenzidine (Sigma, UK) and 0.01% w/v hydrogen peroxide. The analysis of the samples was carried out in an optical microscope (Leica DM4000B, Leica, Germany) and the images were captured with a digital camera (Leica DFC300FX, Leica, Germany). Reaction specificity was confirmed by replacing the specific antibody with normal serum or following pre-absorption of the antiserum with the corresponding antigen.

The staining was evaluated using a computer-based image analysis software (ImageJ, NIH, Bethesda, MD). Col I and OCN staining were measured by applying a fixed threshold to select for positive staining in different bone regions of the femur, both epiphyseal regions and in the diaphysis. Positive pixel area was divided by the total surface bone size. Values were normalized to those measured from SS4W and SS2W groups and reported as relative staining intensities.

In vivo Toxicity

In vivo toxicity was assessed by histological analysis. Liver, kidneys, spleen, lungs, heart and brain were examined for histological signs of toxicity related to the different doses and/or treatment of LPNPs. The organs were prepared for analysis as already described.[28] Briefly, the organs were fixed after extraction by immersion for 24 h in the same fixative and embedded in Paraplast®. Sections of 5 µm thick were obtained, stained with hematoxylin-erythrosine for topographical study and analyzed by light microscopy.

Statistical Analysis

Data are shown as mean ± SEM. Statistical analysis was performed using SPSS 25.0 software. First, the normality and homoscedasticity of the data were checked using the Kolmogorov–Smirnov test and the Levene test, respectively. Statistical differences between two experimental groups were analyzed using Student's *t*-test. Statistical differences

between multiple experimental groups were analyzed with one-way ANOVA followed by post-hoc Tukey's test for multiple comparisons. All tests were performed at a significance level of $\alpha = 0.05$.

Results and Discussion

Lipid-Polymer Hybrid Nanoparticles Characterization

The morphological characteristics of the bare hybrid nanoparticles or functionalized systems, prepared through a microfluidic-based continuous process, are shown in Figure 1.

The obtained LPNPs showed a similar mean diameter than those previously obtained by bulk nanoprecipitation. No significant differences between the different nanoparticle compositions were observed in either of the studied properties (Z-average, PdI and ZP) (Figure 1A). However, a tendency of higher Z-average and PdI after the functionalization with both alendronate and the aptamer in agreement with our previous data was observed.[22] Other authors report the same trend regarding Z-average following a similar strategy of nanoparticles covalent surface functionalization.[29] Moreover, the functionalization with both targeting molecules also led to a lower surface charge indicative of the efficient incorporation of the desired ligands, both depicting a negative charge. This decrease in surface charge could also be useful to increase the colloidal stability of the nanoparticle dispersions. The association efficiency of alendronate was 55.27 ± 3.78%, lower than that previously established for the aptamer covalent attachment (91 ± 2%).[25] However, the use of higher ALD amounts during functionalization will lead to an elevated number of ALD molecules present in the functionalization layer after the reaction compared to Apt modification.

The morphological characteristics of the obtained SFRP1 loaded LPNPs as well as their characterization through NTA are shown in Figure 1B–D. All the systems showed a rounded morphology, as expected. Moreover, despite following the same trend in particle size, the values estimated by NTA are lower than the Z-average values obtained by DLS. These differences can be attributed to the different distribution weighting between both techniques, being considered as complementary methods.[30] On the other hand, the association efficiency of the oligonucleotide, determined on NF-LPNPs, was 82.17 ± 2.40% indicating the high efficiency of the systems to encapsulate GapmeRs and showing higher encapsulation efficiencies than the reported ones for bulk nanoparticle preparation.[22]

A

	Z-average (nm)	PdI	ZP (mV)
NF-LPNPs-SFRP1	190.02 ± 11.63	0.35	-8.82 ± 4.60
ALD-LPNPs-SFRP1	201.62 ± 9.63	0.40	-14.41 ± 4.28
Apt-LPNPs-SFRP1	198.45 ± 7.71	0.38	-21.65 ± 1.76
NF-LPNPs-Cntrl	204.88 ± 12.41	0.33	-10.86 ± 6.65
ALD-LPNPs-Cntrl	206.62 ± 12.51	0.36	-13.97 ± 4.98
Apt-LPNPs-Cntrl	218.80 ± 13.09	0.39	-20.52 ± 3.22

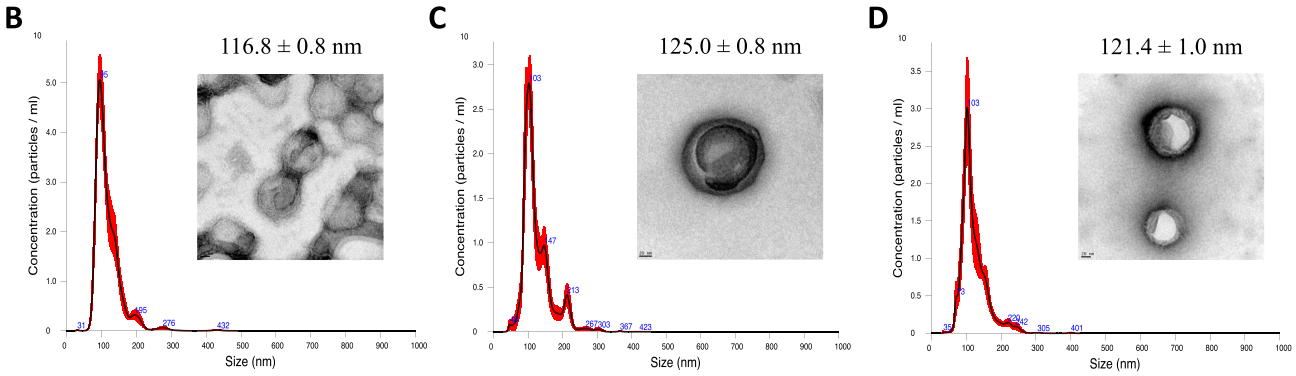

Figure 1 Physicochemical properties of the developed nanoparticles by DLS ((**A**) n = 8), NTA and TEM (**B-D**). (**B**) NF-LPNPs-SFRP1; (**C**) ALD-LPNPs-SFRP1; (**D**) Apt-LPNPs-SFRP1. Scale bar 20 nm.

According to the obtained experimental results, no significant differences were found between the formulations, allowing us to analyze the differences between their bone induction capacity based on the targeting strategy followed and the dose administered.

Trabecular Bone Quality by Histomorphometrical and Micro-CT Analysis

The obtained functionalized and non-functionalized nanoparticles loaded either with the therapeutic (SFRP1) or control GapmeR were administered at three doses, namely low (equivalent 75 ng of GapmeR), intermediate (equivalent 150 ng of GapmeR) and high (equivalent 300 ng of GapmeR). Bone architecture analysis of the treated mice was performed by histology and histomorphometrical assessments, as well as by micro-computed tomography (micro-CT). The use of both techniques is complementary and could provide both two-dimensional and three-dimensional evaluations.[31] The histological analysis of the femur samples showed a preserved tissue architecture in all experimental groups with slight differences at the cellular level (Figure 2). These differences were mainly reflected in the degree of hypertrophy of some groups of osteoblasts in specific areas of the bone as shown in Figure S1. The osteoblasts that showed a more hypertrophic morphology, indicative of biosynthetic activity, were located mainly in areas of the diaphyseal cortical bone surface. The results observed were similar within the different doses tested.

The histomorphometric analysis of the three parameters evaluated in the trabecular bone structure showed significant differences in the trabecular width (Tb.Wi) and number (Tb.N) ($p < 0.05$). Specifically, Tb.Wi (Figure 3A) of mice treated with Apt-LPNPs-SFRP1 at the low dose (75 ng GapmeR) showed significant differences with respect to the saline solution group (SS4W) ($p < 0.05$). Mice treated with the intermediate dose of LPNPs loaded with the SFRP1 GapmeR (150 ng GapmeR) and functionalized with alendronate or aptamer showed by histology significantly higher Tb.Wi than mice treated with the saline solution (SS) and the corresponding nanoparticles with control GapmeR (ALD-LPNPs-Cntrl and Apt-LPNPs-Cntrl, respectively) ($p < 0.05$). The micro-CT assessment confirmed the higher Tb.Wi for the ALD-LPNPs-SFRP1 ($p < 0.05$) at the intermediate dose (Figure 3B). At the high dose (300 ng GapmeR), mice treated with NF-LPNP-SFRP1 and ALD-LPNPs-SFRP1 showed significantly higher Tb.Wi compared to the SS, whereas Apt-LPNPs-SFRP1 treated mice showed an increased Tb.Wi compared to SS and the Apt-LPNPs-Cntrl ($p < 0.05$). These results are consistent with our previous data for Apt-LPNPs-SFRP1 prepared by bulk precipitation and administered at the equivalent low dose of this study where higher Tb.Wi was observed for the group treated with the therapeutic nanoparticles compared to the control group (SS).[22]

The histomorphometric parameter trabecular separation (Tb.Sp) did not show significant statistical differences between any of the analyzed groups neither by histology (Figure 3C) nor by micro-CT analysis (Figure 3D). Regarding trabecular number (Tb.N) (Figure 3E), at the low dose groups (75 ng GapmeR) mice treated with Apt-LPNPs-SFRP1 showed a statistically higher Tb.N, compared to saline solution (SS4W) and Apt-LPNPs-Cntrl ($p < 0.05$). At the intermediate dose (150 ng GapmeR) and high (300 ng GapmeR) dose, mice treated with ALD-LPNPs-SFRP1 and Apt-LPNPs-SFRP1 showed higher Tb.N than SS (SS2W) and the corresponding functionalized nanoparticles loaded with the control GapmeR (ALD-LPNPs-Cntrl or Apt-LPNPs-Cntrl, respectively) ($p < 0.05$). Regarding non-functionalized nanoparticles, only the intermediate dose incorporating the SFRP1 GapmeR (NF-LPNPs-SFRP1) showed significant differences with respect to the SS group (SS2W) ($p < 0.05$). On the other hand, the quantification by micro-CT only showed significant differences in Tb.N for mice treated with ALD-LPNPs-SFRP1 at the highest dose (300 ng) compared to the SS control (SS2W) ($p < 0.05$) (Figure 3F).

Moreover, there are additional parameters such as bone mineral density (BMD), indicative of bone strength, and the relationship between bone volume/total volume (BV/TV) that require estimation of volumes, and, therefore, three-dimensional determinations. The use of micro-CT analysis allows for the visualization of the 3D structure of the reconstructed scans showed in Figure 4A for the high dose treated mice. The obtained values of trabecular BMD showed that, at the low dose, mice treated with SS depicted lower BMD ($p < 0.05$) compared to all the groups except for ALD-LPNPs-Cntrl (Figure 4B). Moreover, when the mice were treated with the highest dose of ALD-LPNPs-SFRP1 they showed a higher BMD compared to saline solution, NF-LPNPs-Cntrl and ALD-LPNPs-Cntrl groups ($p < 0.05$) at the same dose indicating an induction in bone formation. Additionally, the same treatment group at the same dose also showed a significant increase ($p < 0.05$) in the BV/TV ratio when compared to saline solution control and NF-LPNPs-

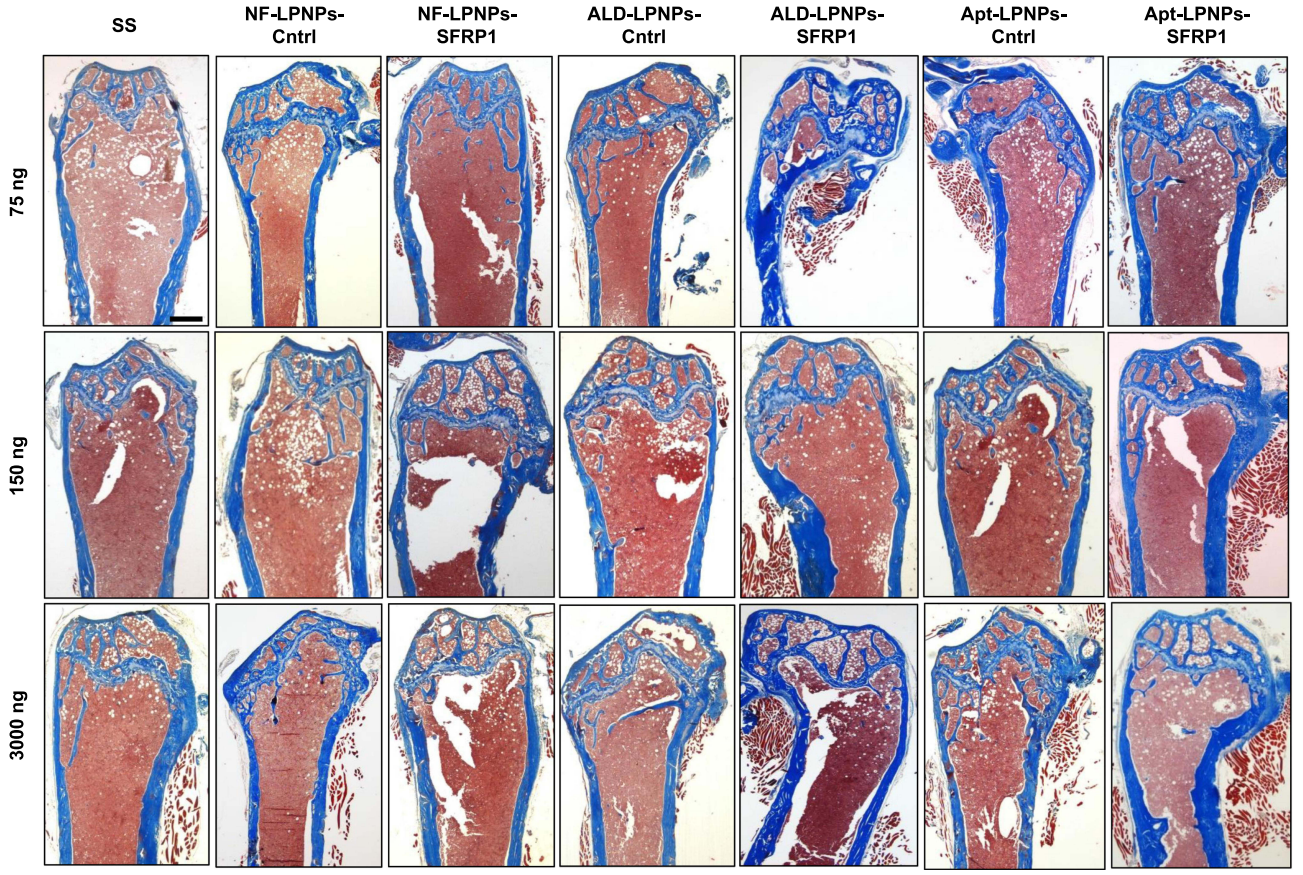

Figure 2 Representative panoramic images of the femur in longitudinal section stained with Masson-Trichrome showing the bone microarchitecture in all the experimental groups treated with the three different doses (75, 150 and 300 ng). SS corresponds to saline solution administration once every 4 weeks or once every 2 weeks (SS4W (75 ng) and SS2W (150 and 300 ng)). Scale bar: 0.5 mm.

Cntrl (Figure 4C). Interestingly, this treatment led to a statistically higher BV/TV (%) than the saline solution control also at the low and intermediate doses ($p < 0.05$).

Taking together the results regarding trabecular bone morphology, this study shows that mice treated with ALD-LPNPs-SFRP1 exhibited an enhanced bone quality. Furthermore, a dose-dependent relationship is evident within this group, wherein the magnitude of observed morphological changes correlates with the administered GapmeR dose. Specifically, at least an intermediate dose is requisite for augmenting trabecular bone width and number. Notably, a significant increase in BMD and BV/TV are only observed following administration of the highest dose (300 ng GapmeR) ($p < 0.05$). Although the analysis of a dose–response effect of gene silencing on bone quality has not been described, prior research on miRNA and siRNA-loaded liposomes and lipid nanoparticles has reported a threshold. Above this threshold, a consistent silencing effect has been observed in studies evaluating in vivo silencing efficiency.[20,32]

Cortical Bone Quality by Histomorphometrical and Micro-CT Analysis

Despite bone osteoporosis is known to affect both trabecular and cortical bone, it has been described that the highest bone mass loss in established osteoporosis takes place in the cortical region through an enhanced intracortical remodeling.[33] This phenomenon is related to an increased porosity of the cortical bone and a decrease in cortical bone thickness.[34] Remarkably, the parameter of bone quality that exhibited the most pronounced disparities, as revealed through histomorphometric assessments and micro-CT analysis, was the width of the cortical bone in the diaphysis (Ct.Wi) (Figure 5). Mice treated with ALD-LPNPs-SFRP1 at the intermediate (150 ng GapmeR) and high dose (300 ng GapmeR) showed the highest Ct.Wi with values significantly higher than mice treated with saline solution and ALD-LPNPs-Cntrl based on the histological analysis ($p < 0.05$). Moreover, NF-LPNPs-SFRP1 and Apt-LPNPs-SFRP1 treated mice also at

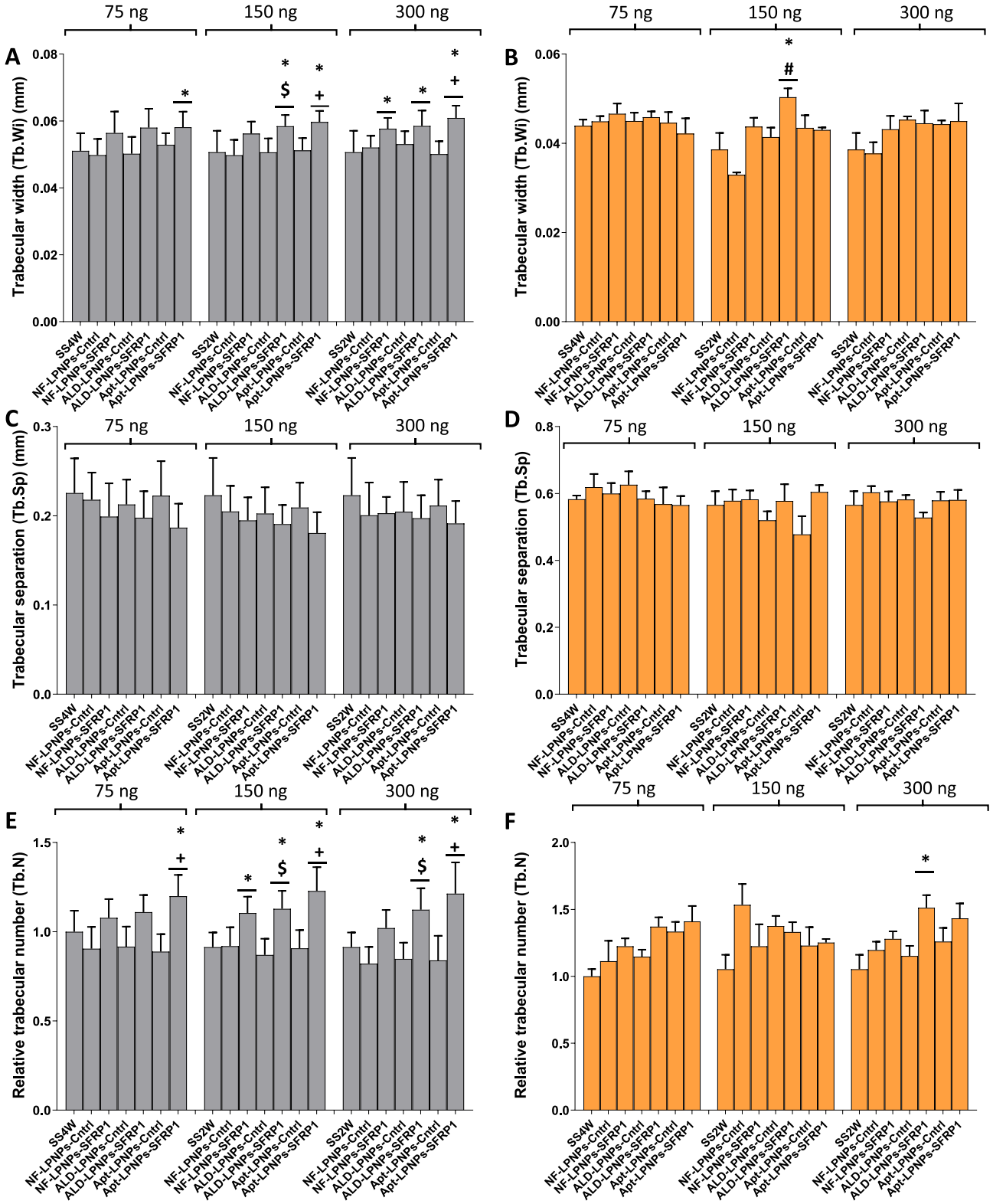

Figure 3 Trabecular bone quality parameters (Trabecular width (Tb.Wi), Trabecular separation (Tb.Sp) and Trabecular number (Tb.N)) determined in 2D by histomorphometric assessments (**A, C, E**) and in 3D by micro-CT (**B, D, F**). (*) denotes significant differences with the corresponding control (saline solution) ($p<0.05$). (#) denotes statistically significant differences to NF-LPNPs-Cntrl with the corresponding dose ($p<0.05$). ($) denotes statistically significant differences to ALD-LPNPs-Cntrl with the corresponding dose ($p<0.05$). (+) denotes statistically significant differences to Apt-LPNPs-Cntrl with the corresponding dose ($p<0.05$).

https://doi.org/10.2147/IJN.S476546 DovePress

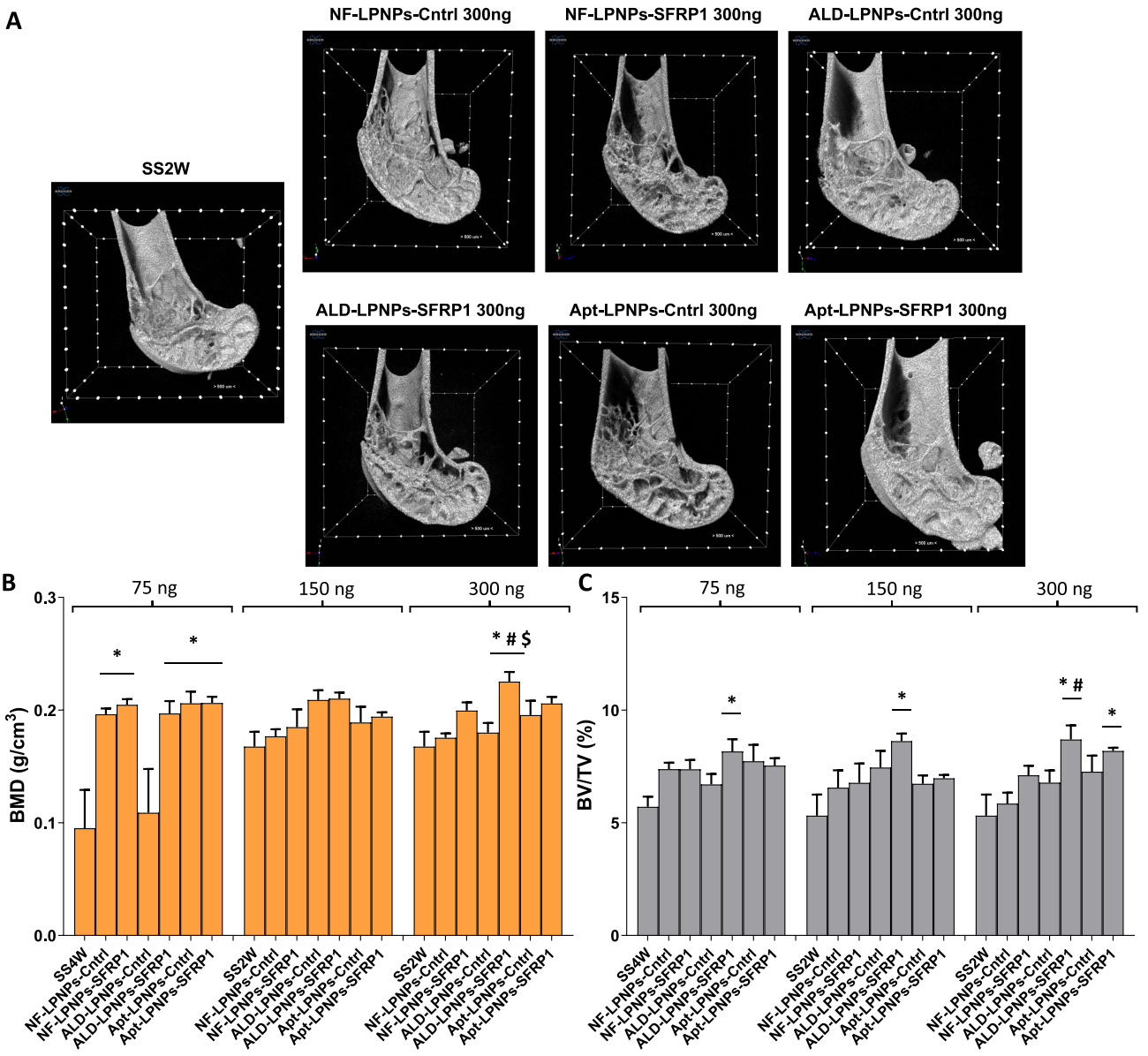

Figure 4 (**A**) Representative images of the micro-CT reconstruction of the groups treated with the higher dose. (**B and C**) Bone quality parameters determined by micro-CT. (*) denotes statistically significant differences with the corresponding control (saline solution) ($p<0.05$). (#) denotes statistically significant differences to NF-LPNPs-Cntrl with the corresponding dose ($p<0.05$). ($) denotes statistically significant differences to ALD-LPNPs-Cntrl with the corresponding dose ($p<0.05$).

the intermediate and high doses showed significantly higher Ct.Wi compared to the saline solution control and nanoparticles loaded with the control GapmeR (NF-LPNPs-Cntrl and Apt-LPNPs-Cntrl), respectively ($p < 0.05$). No differences were observed when comparing the same formulations at different doses. Histological assessments are the gold standard method to evaluate bone architecture. Despite other reports indicate a good correlation between the cortical morphological parameters obtained by histology and micro-CT for Haversian canal separation, Haversian canal diameter and cortical porosity, this study highlighted that histology is able to point out higher differences in cortical bone width between the treatment groups.[35] Among the differences between trabecular and cortical bone remodeling levels and mechanical properties stand out. In fact, modifications in the Wnt/β-catenin signaling pathway have been shown to exert different effects in trabecular and cortical bone.[36] These differences could explain the higher effect observed for the nanoparticles in the cortical bone compared to trabecular bone.

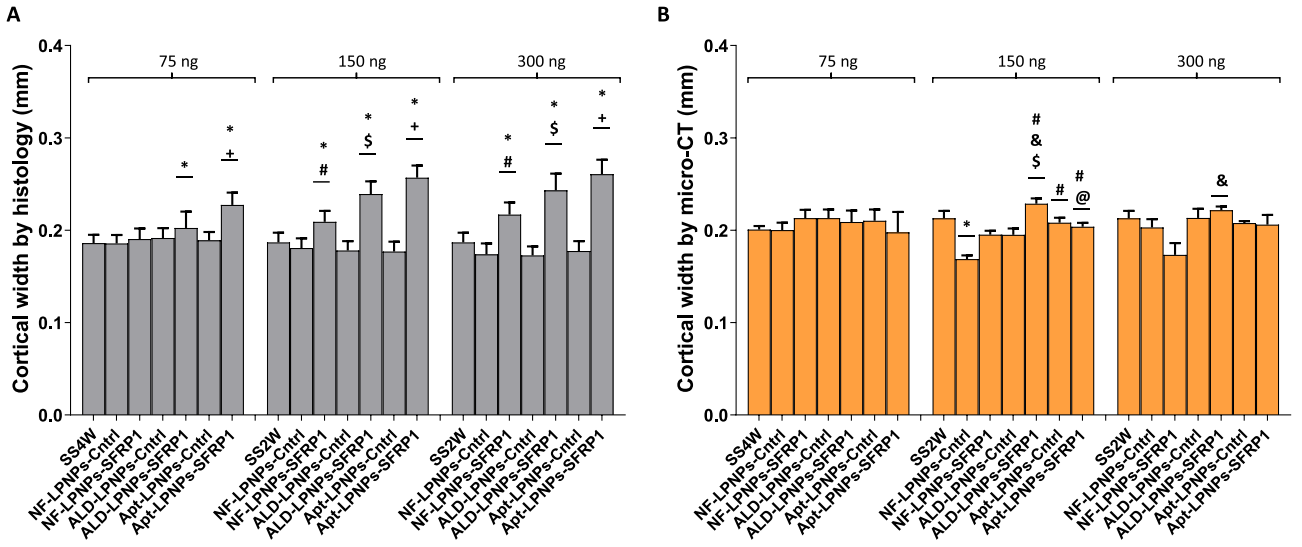

Figure 5 Cortical width of the different treatment groups by histology (**A**) and micro-CT (**B**) assessments. (*) denotes statistically significant differences with the corresponding control (saline solution) ($p<0.05$). (#) denotes statistically significant differences to NF-LPNPs-Cntrl with the corresponding dose ($p<0.05$). (and) denotes statistically significant differences to NF-LPNPs-SFRP1 with the corresponding dose ($p<0.05$). ($) denotes statistically significant differences to ALD-LPNPs-Cntrl with the corresponding dose ($p<0.05$). (@) denotes statistically significant differences to ALD-LPNPs-SFRP1 with the corresponding dose ($p<0.05$). (+) denotes statistically significant differences to Apt-LPNPs-Cntrl with the corresponding dose ($p<0.05$).

Immunohistochemical Analysis

The immunohistochemical analysis of collagen type I (Col I), a marker of early osteogenesis, and osteocalcin (OCN), a marker of late osteogenesis and mineralization, showed similar relative staining intensity values of both markers in most of the experimental groups (Figure 6). Among the groups evaluated, only those administered nanoparticles encapsulating the SFRP1 GapmeR and aptamer-functionalized at all three tested doses (Apt-LPNPs-SFRP1), along with alendronate at the intermediate and high doses (150 ng and 300 ng of ALD-LPNPs-SFRP1), demonstrated elevated relative staining intensity values for both markers compared to the SS, NF-LPNPs-Cntrl, NF-LPNPs-SFRP1, ALD-LPNPs-Cntrl, and Apt-LPNPs-Cntrl groups ($p < 0.05$). The increase in the expression of both proteins is a sign of good-quality bone formation. In this sense, the expression of Col I and OCN showing how the groups treated with SFRP1 loaded nanoparticles functionalized with aptamer at the three doses and with alendronate at the intermediate and high doses, showing a higher level of relative intensity, which suggests formation of better-quality bone, both structurally and functionally. Although the staining intensity quantification was performed on the overall bone surface, cortical bone primarily contributes to the total mass of the femur. This could explain the observed direct correlation between the cortical width and the expression levels of both osteogenic markers, Col I and OCN.

Bone marrow MSCs play a crucial role in the modulation of bone remodeling, both at the trabecular and cortical level.[37] The use of ASOs to modulate their commitment and induce their differentiation towards osteoblasts can be a strategy to control bone remodeling. By modulating the WNT/β-catenin pathway though the SFRP1 silencing the developed nanoparticles, specifically, the ones functionalized with the aptamer and alendronate, were able to reverse bone remodeling, promoting osteosynthesis and improving the histomorphometric parameters at both the trabecular bone and the cortical bone level. This effect may be associated with the efficient induction of osteoblast formation. Additionally, the more pronounced effects observed in cortical bone could be related to the different inherent metabolic activity of both regions of the tissue. Moreover, it has been previously reported that different WNT/β-catenin pathway modulators can induce different responses in trabecular and cortical bone depending on the specific mediator.[38,39] The achieved effect of enhanced cortical bone width will be highly beneficial for osteoporosis management, decreasing the risk of fragility fractures. These types of fractures reduce the patient's quality of life, disability and mortality.[40]

Moreover, the functionalization of the developed nanoparticles through covalent bonding using two bone-targeting strategies led to the specific delivery of the oligonucleotide to the bone tissue. These systems outperformed the non-

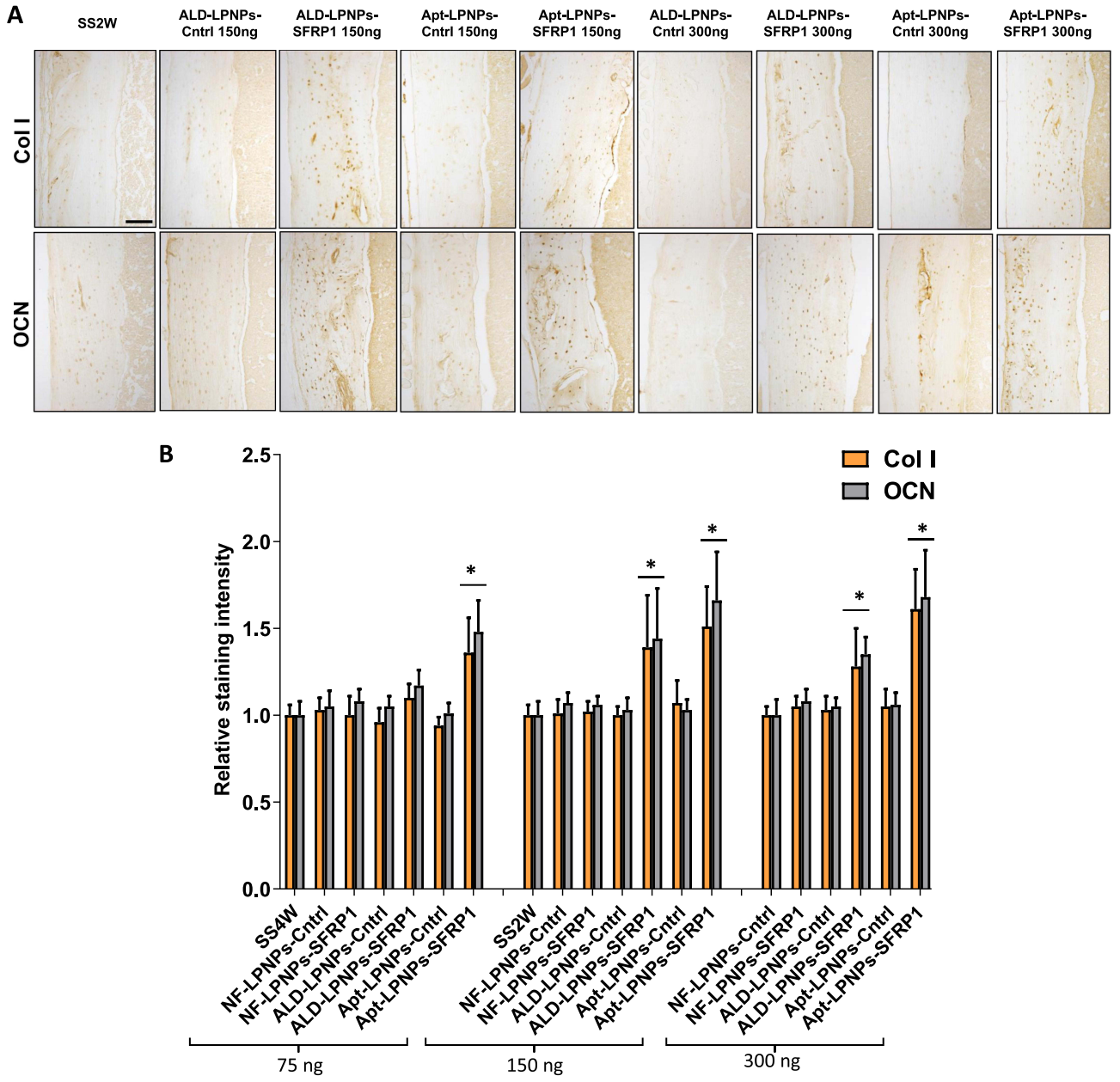

Figure 6 (**A**) Semi-panoramic images of diaphyseal cortical bone femur showing the presence of Col I and OCN immunoreactivity in the control (SS2W) and LPNPs treated experimental groups with GapmeR Control (NF-LPNPs-Cntrl, ALD-LPNPs-Cntrl and Apt-LPNPs-Cntrl) or therapeutic GapmeR (NF-LPNPs-SFRP1, ALD-LPNPs-SFRP1, Apt-LPNPs-SFRP1) corresponding to the intermediate (150 ng) and high (300 ng) doses that show better histomorphometric characteristics. (**B**) Graphs showing the relative staining intensity of Col I and OCN in the LPNPs treated experimental groups (NF-LPNPs-Cntrl, NF-LPNPs-SFRP1, ALD-LPNPs-Cntrl, ALD-LPNPs-SFRP1, Apt-LPNPs-Cntrl and Apt-LPNPs-SFRP1) and controls, saline solution administration once every 4 weeks or once every 2 weeks (SS4W and SS2W). Histograms represent mean ± SD values. (*) denotes statistically significant differences to corresponding saline solution ($p<0.05$). Scale bar: 60μm.

functionalized nanoparticles that, even loaded with the same amount of the oligonucleotide, failed to promote an improvement in the bone histomorphometric parameters. Therefore, as previously described by other authors, the efficient delivery of the oligonucleotides is crucial not only to endow their cargo with tissue specificity and reduce systemic toxic effects but also to ensure their therapeutic effect.[41] Interestingly, while the treatment of osteoporotic mice with ALD-LPNPs-SFRP1 seems to follow a dose-dependent effect requiring at least a 150 ng GapmeR dose to promote an enhancement in the bone quality parameters, this effect is not observed for Apt-LPNPs-SFRP1. These differences could be explained by the different targeting strategy followed that would modify the affinity of the LPNPs for the different tissue components. ALD functionalization will induce LPNPs accumulation at the bone surface driven by the

affinity of ALD for hydroxyapatite.[42] On the other hand, Apt functionalized LPNPs will induce a more efficient cell uptake due to their affinity for the cell membrane.[22] Therefore, all the concentrations tested for Apt-LPNPs-SFRP1 could be above the required threshold to obtain a good silencing while for ALD-LPNPs-SFRP1 the threshold is above 75 ng dose. Moreover, these different LPNPs distributions within the tissue could also explain the differences observed in bone quality parameters between both targeting strategies.

Toxicity Assessment

Microscopic analysis showed non-significant differences in the organs of animals treated with the different nanoparticle formulations assayed: NF-LPNPs-Cntrl, NF-LPNPs-SFRP1, ALD-LPNPs-Cntrl, ALD-LPNPs-SFRP1, Apt-LPNPs-Cntrl and Apt-LPNPs-SFRP1 at any of the GapmeR doses (75, 150 and 300 ng) with respect to the organs of the control groups (SS2W and SS4W). However, small changes at the cellular level were observed in the liver and kidney in both treated and control animals because of histological processing, and an isolated finding was observed in the lung of one of the control animals.

Representative images of the higher dose treatments (300 ng) are only shown as no differences were observed with the lower doses (Figure 7). Moreover, more details regarding specific histology changes are included in Figure S2. The

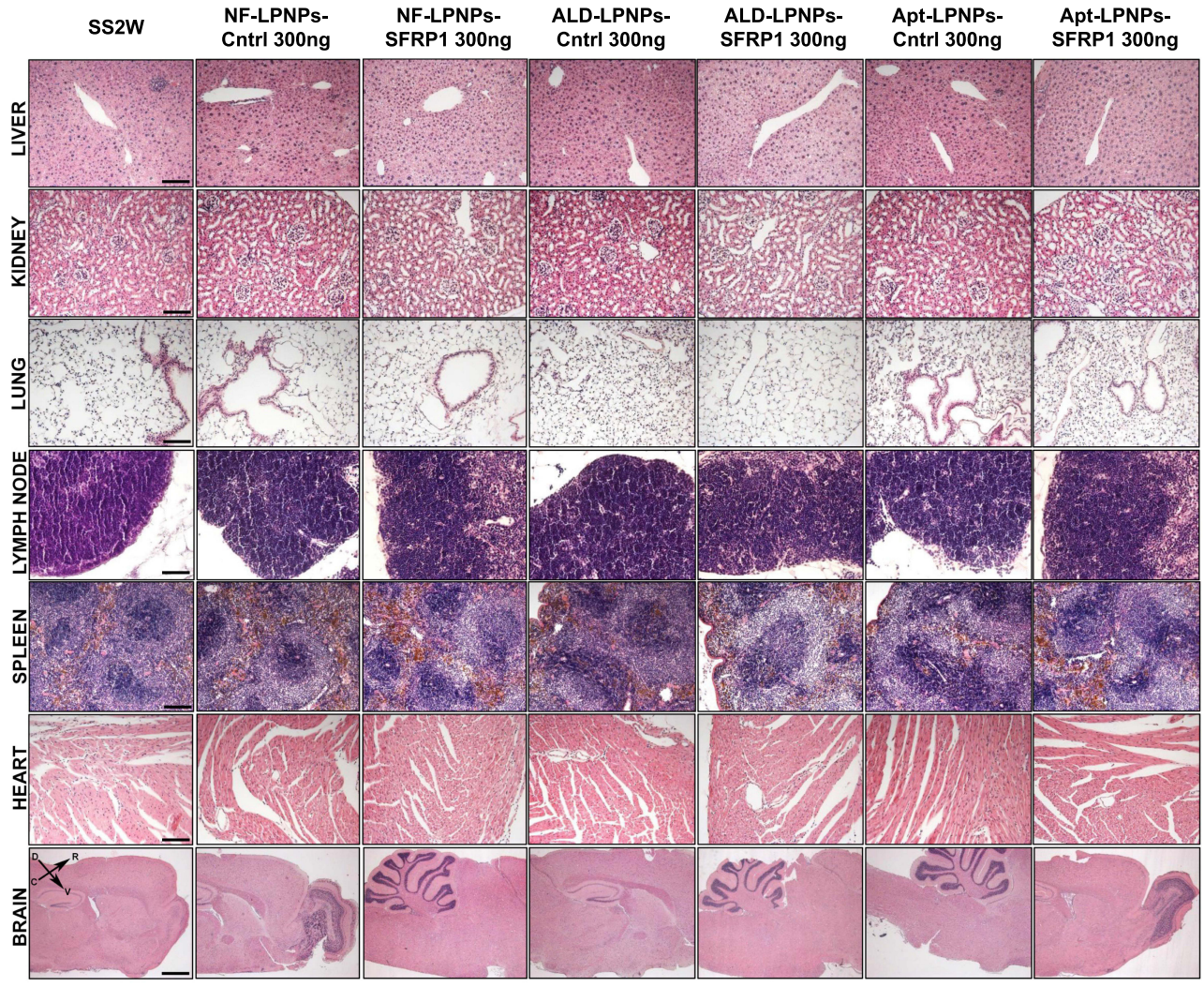

Figure 7 Representative semi-panoramic images in the controls and treated experimental groups with high doses (300 ng) showing the histological structure of the liver, kidney, lung, lymph node, spleen, heart and brain. All the organs analyzed show normal tissue architecture with no apparent changes at the cellular level. Scale bars: liver, kidney, lung, lymph node, spleen and heart: 120 µm; brain: 300 µm.

global analysis showed the liver presented a normal tissue structure with hepatocytes arranged in cords around sinusoid capillaries of normal size and morphology. The vascular spaces of portal and hepatic systems presented normal size and morphology as well as the bile ducts, however all the animals presented some reactive changes in hepatocyte nuclei and isolated groups of inflammatory cells in different regions of the liver parenchyma in both control (SS2W) and treated animals.

The kidney showed a normal tissue structure both in cortex and medulla, observing renal corpuscles of normal size and morphology in which the flat epithelium of Bowman's capsule is observed. The proximal convoluted tubules dominated the parenchyma of renal cortex, showing the characteristic cubic epithelium of intense eosinophilic stain and the brush border in the apical domain of epithelial cells. Some unspecific and non-significant changes were observed at the cellular level in the liver and kidney, in most animals, both in the treated and control groups. These changes consisted of slight reactive changes at the nuclear level, reflected in more intensely basophilic nuclei and the presence of some hepatocytes and tubular epithelial cells with barely eosinophilic cytoplasm (Figure S2).

The lung showed normal tissue structure without significant changes or signs of fibrosis. Air spaces, alveolar and pulmonary sacs presented normal structure without significant changes and no thickening of the walls. Vascular spaces of normal size and morphology were observed. In most animals from both SFRP1 GapmeR and Cntrl GapmeR groups, clusters of lymphoid cells and isolated macrophages containing lipofuscin were observed around some blood vessels. A distinct alteration was observed in one of the animals from ALD-LPNPs-Cntrl 150 ng group that presented a proliferative lesion proximal to the hilum in the right lung (Figure S2). Subsequent examination revealed a benign bronchiolar adenoma.

The lymph nodes of the inguinal and popliteal regions presented a structure and cellular composition consistent with physiological parameters. The spleen also showed a normal tissue structure without significant changes in cell composition and distribution, clearly observing the differentiation between white pulp and red pulp.

The heart presented, in all groups, a normal histological structure without significant changes. The myocardium showed cardiomyocytes with preserved morphology, showing nuclei in central position and intercalary discs in normal proportion.

The brain presented a normal histological structure in rostral and caudal areas, without significant changes in the distribution of gray and white matter. Ventricles of preserved size and morphology were also observed in which choroid plexuses of normal structure could be identified.

Despite observing some immune cell infiltration in both control and LPNPs treated groups, no toxic events related to the nanoparticles administration were observed.

Conclusions

In this study, we successfully developed a microfluidic-based approach for the continuous synthesis of hybrid lipid-polymer nanoparticle systems. The developed nanoparticles showed high oligonucleotide association efficiency and an enhanced ability to target bone via two distinct strategies: alendronate and aptamer surface functionalization. Following the administration of nanoparticles via the tail vein of osteoporotic mice, histological and microCT evaluations after 3 months revealed a significant improvement in bone trabecular microarchitecture in mice treated with ALD-LPNPs-SFRP1. Cortical bone assessments revealed an improved cortical width of mice treated with both bone-targeted nanoparticles, Apt-LPNPs-SFRP1 and ALD-LPNPs-SFRP1, also depicting higher expression of Col I and OCN. Moreover, no toxicity effects were observed in major organs at every dose studied, indicating the lack of any relevant toxicity of the treatments. Furthermore, a dose–response relationship was observed, with intermediate to high doses of up to 300 ng of GapmeR resulting in enhanced cortical and trabecular bone quality in animals treated with ALD-LPNPs-SFRP1. These results highlighted the need to establish an appropriate dosage regimen to ensure an optimal therapeutic response and point out novel strategies to improve cortical bone quality in osteoporosis by decreasing the risk of fragility fractures.

The study presents limitations, such as a limited range of dosage regimens. Moreover, the lack of longer follow-up limits the understanding of the sustained effects on bone regeneration.

Future research should consider optimizing dosage regimens for gene therapy delivery systems to maximize therapeutic efficacy while minimizing side effects. Also, exploring alternative functionalization strategies in preclinical models may enhance the impact of the treatments in potential osteoporosis treatment.

Funding

This work was supported by the Spanish Ministry of Science and Innovation (MCIN/AEI/10.13039/501100011033/FEDER, UE, PID2021-127493OB-C21 and PID2021-127493OA-C22). E.B. thanks the Canary Islands Agency for Research, Innovation and Information Society (ACIISI) of the Counseling of Economy, Knowledge and Employment and the European Social Fund (ESF) Integrated Operational Program of the Canary Islands 2014–2020 for his predoctoral grant (TESIS2022010094).

Disclosure

The authors report no conflicts of interest in this work.

References

1. Ayub N, Faraj M, Ghatan S, Reijers JA, Napoli N, Oei L. The treatment gap in osteoporosis. *J Clin Med*. 2021;10(13):3002. doi:10.3390/jcm10133002
2. Hernlund E, Svedbom A, Ivergård M, et al. Osteoporosis in the European Union: medical management, epidemiology and economic burden: a report prepared in collaboration with the International Osteoporosis Foundation (IOF) and the European Federation of Pharmaceutical Industry Associations (EFPIA). *Archiv Osteoporosis*. 2013;8(1–2):1. doi:10.1007/s11657-013-0136-1.
3. Cheung WH, Miclau T, Chow SK-H, Yang FF, Alt V. Fracture healing in osteoporotic bone. *Injury*. 2016;47(S21–S6):S21–S26. doi:10.1016/S0020-1383(16)47004-X
4. von Rüden C, Augat P. Failure of fracture fixation in osteoporotic bone. *Injury*. 2016;47:S3–S10. doi:10.1016/S0020-1383(16)47002-6
5. Foulke BA, Kendal AR, Murray DW, Pandit H. Fracture healing in the elderly: a review. *Maturitas*. 2016;92:49–55. doi:10.1016/j.maturitas.2016.07.014
6. Marin C, Luyten FP, Van der Schueren B, Kerckhofs G, Vandamme K. The Impact of Type 2 Diabetes on Bone Fracture Healing. *Front Endocrinol*. 2018;9. doi:10.3389/fendo.2018.00006
7. Burrus MT, Werner BC, Yarboro SR. Obesity is associated with increased postoperative complications after operative management of tibial shaft fractures. *Injury*. 2016;47(2):465–470. doi:10.1016/j.injury.2015.10.026
8. Patel D, Wairkar S. Bone regeneration in osteoporosis: opportunities and challenges. *Drug Delivery Transl Res*. 2023;13(2):419–432. doi:10.1007/s13346-022-01222-6
9. Rouco H, García-García P, Briffault E, Diaz-Rodriguez P. Modulating osteoclasts with nanoparticles: a path for osteoporosis management? *Wiley Interdiscip Rev Nanomed Nanobiotechnol*. 2023;15(4):e1885. doi:10.1002/wnan.1885
10. Iolascon G, Moretti A, Toro G, Gimigliano F, Liguori S, Paoletta M. Pharmacological Therapy of Osteoporosis: what's New? *Clin Interv Aging*. 2020;15:485–491. doi:10.2147/CIA.S242038
11. Johannes L, Lucchino M. Current Challenges in Delivery and Cytosolic Translocation of Therapeutic RNAs. *Nucleic Acid Therap*. 2018;28(3):178–193. doi:10.1089/nat.2017.0716
12. Manolagas SC. Wnt signaling and osteoporosis. *Maturitas*. 2014;78(3):233–237. doi:10.1016/j.maturitas.2014.04.013
13. Yu T, Wang H, Zhang Y, Wang X, Han B. The Delivery of RNA-Interference Therapies Based on Engineered Hydrogels for Bone Tissue Regeneration. *Front Bioeng Biotechnol*. 2020;8:445. doi:10.3389/fbioe.2020.00445
14. Oh W-T, Yang Y-S, Xie J, et al. WNT-modulating gene silencers as a gene therapy for osteoporosis, bone fracture, and critical-sized bone defects. *Mol Ther*. 2023;31(2):435–453. doi:10.1016/j.ymthe.2022.09.018
15. Yang Y-S, Xie J, Wang D, et al. Bone-targeting AAV-mediated silencing of Schnurri-3 prevents bone loss in osteoporosis. *Nat Commun*. 2019;10(1):2958. doi:10.1038/s41467-019-10809-6
16. Cui Y, Guo Y, Kong L, et al. A bone-targeted engineered exosome platform delivering siRNA to treat osteoporosis. *Bioact Mater*. 2022;10:207–221. doi:10.1016/j.bioactmat.2021.09.015
17. Guo J, Wang F, Hu Y, et al. Exosome-based bone-targeting drug delivery alleviates impaired osteoblastic bone formation and bone loss in inflammatory bowel diseases. *Cell Rep Med*. 2023;4(1):100881. doi:10.1016/j.xcrm.2022.100881
18. Mora-Raimundo P, Lozano D, Benito M, Mulero F, Manzano M, Vallet-Regí M. Osteoporosis Remission and New Bone Formation with Mesoporous Silica Nanoparticles. *Adv Sci*. 2021;8(16):e2101107. doi:10.1002/advs.202101107
19. Liu J, Zhang Y, Wu Y, et al. Delivery of m7G methylated Runx2 mRNA by bone-targeted lipid nanoparticle promotes osteoblastic bone formation in senile osteoporosis. *Nano Today*. 2024;54:102074. doi:10.1016/j.nantod.2023.102074
20. Liu J, Dang L, Li D, et al. A delivery system specifically approaching bone resorption surfaces to facilitate therapeutic modulation of microRNAs in osteoclasts. *Biomaterials*. 2015;52:148–160. doi:10.1016/j.biomaterials.2015.02.007
21. Zhang Y, Wei L, Miron RJ, Shi B, Bian Z. Anabolic Bone Formation Via a Site-Specific Bone-Targeting Delivery System by Interfering With Semaphorin 4d Expression. *J Bone Miner Res*. 2015;30(2):286–296. doi:10.1002/jbmr.2322
22. García-García P, Reyes R, García-Sánchez D, et al. Nanoparticle-mediated selective Sfrp-1 silencing enhances bone density in osteoporotic mice. *J Nanobiotechnol*. 2022;20(1):462. doi:10.1186/s12951-022-01674-5
23. Claudel M, Jouzeau J-Y, Cailotto F. Secreted Frizzled-related proteins (sFRPs) in osteo-articular diseases: much more than simple antagonists of Wnt signaling? *FEBS J*. 2019;286(24):4832–4851. doi:10.1111/febs.15119
24. Jing C, Li B, Tan H, et al. Alendronate-Decorated Nanoparticles as Bone-Targeted Alendronate Carriers for Potential Osteoporosis Treatment. *ACS Appl Bio Mater*. 2021;4(6):4907–4916. doi:10.1021/acsabm.1c00199
25. Rouco H, García-García P, Évora C, Díaz-Rodríguez P, Delgado A. Screening strategies for surface modification of lipid-polymer hybrid nanoparticles. *Int J Pharm*. 2022;624:121973. doi:10.1016/j.ijpharm.2022.121973

26. Garcia-Garcia P, Reyes R, Rodriguez JA, et al. The Bone Regeneration Capacity of BMP-2 + MMP-10 Loaded Scaffolds Depends on the Tissue Status. *Pharmaceutics*. 2021;13(7):979. doi:10.3390/pharmaceutics13070979
27. Gage GJ, Kipke DR, Shain W. Whole Animal Perfusion Fixation for Rodents. *JoVE*. 2012;2012(65):e3564.
28. Hernández A, Sánchez E, Soriano I, Reyes R, Delgado A, Évora C. Material-related effects of BMP-2 delivery systems on bone regeneration. *Acta Biomater*. 2012;8(2):781–791. doi:10.1016/j.actbio.2011.10.008
29. Chen Q, Zheng C, Li Y, et al. Bone Targeted Delivery of SDF-1 via Alendronate Functionalized Nanoparticles in Guiding Stem Cell Migration. *ACS Appl Mater Interfaces*. 2018;10(28):23700–23710. doi:10.1021/acsami.8b08606
30. Kim A, Ng WB, Bernt W, Cho N-J. Validation of Size Estimation of Nanoparticle Tracking Analysis on Polydisperse Macromolecule Assembly. *Sci Rep*. 2019;9(1):2639. doi:10.1038/s41598-019-38915-x
31. Bernhardt R, Kuhlisch E, Schulz MC, Eckelt U, Stadlinger B. Comparison of bone-implant contact and bone-implant volume between 2D-histological sections and 3D-SRµCT slices. *Eur Cells Mater*. 2012;23:237–47;discussion47–8. doi:10.22203/eCM.v023a18
32. Lokugamage MP, Sago CD, Gan Z, Krupczak BR, Dahlman JE. Constrained Nanoparticles Deliver siRNA and sgRNA to T Cells In Vivo without Targeting Ligands. *Adv Mater*. 2019;31(41):e1902251. doi:10.1002/adma.201902251
33. Osterhoff G, Morgan EF, Shefelbine SJ, Karim L, McNamara LM, Augat P. Bone mechanical properties and changes with osteoporosis. *Injury*. 2016;47(Suppl 2):S11–20. doi:10.1016/S0020-1383(16)47003-8
34. Chen H, Zhou X, Fujita H, Onozuka M, Kubo KY. Age-related changes in trabecular and cortical bone microstructure. *Int J Endocrinol*. 2013;2013:213234. doi:10.1155/2013/213234
35. Particelli F, Mecozzi L, Beraudi A, Montesi M, Baruffaldi F, Viceconti M. A comparison between micro-CT and histology for the evaluation of cortical bone: effect of polymethylmethacrylate embedding on structural parameters. *J Microsc*. 2012;245(3):302–310. doi:10.1111/j.1365-2818.2011.03573.x
36. Li J, Bao Q, Chen S, et al. Different bone remodeling levels of trabecular and cortical bone in response to changes in Wnt/β-catenin signaling in mice. *J Orthop Res*. 2017;35(4):812–819. doi:10.1002/jor.23339
37. Wang L, You X, Zhang L, Zhang C, Zou W. Mechanical regulation of bone remodeling. *Bone Res*. 2022;10(1):16. doi:10.1038/s41413-022-00190-4
38. Movérare-Skrtic S, Henning P, Liu X, et al. Osteoblast-derived WNT16 represses osteoclastogenesis and prevents cortical bone fragility fractures. *Nat Med*. 2014;20(11):1279–1288. doi:10.1038/nm.3654
39. Maeda K, Kobayashi Y, Udagawa N, et al. Wnt5a-Ror2 signaling between osteoblast-lineage cells and osteoclast precursors enhances osteoclastogenesis. *Nat Med*. 2012;18(3):405–412. doi:10.1038/nm.2653
40. Dimai HP, Fahrleitner-Pammer A. Osteoporosis and Fragility Fractures: currently available pharmacological options and future directions. *Best Pract Res*. 2022;36(3):101780. doi:10.1016/j.berh.2022.101780
41. Tietjen GT, Bracaglia LG, Saltzman WM, Pober JS. Focus on Fundamentals: achieving Effective Nanoparticle Targeting. *Trends Mol Med*. 2018;24(7):598–606. doi:10.1016/j.molmed.2018.05.003
42. Wang Y, Yao J, Cai L, et al. Bone-Targeted Extracellular Vesicles from Mesenchymal Stem Cells for Osteoporosis Therapy. *Int J Nanomed*. 2020;15:7967–7977. doi:10.2147/IJN.S263756